Desalination and Water Treatment
www.deswater.com

doi: 10.5004/dwt.2019.24013

155 (2019) 350–363
July

Synthesis of α-cellulose/magnetite/polypyrrole composite for the removal of reactive black 5 dye from aqueous solutions

Paola E. Díaz-Flores[a], Camerina J. Guzmán-Álvarez[b], Víctor M. Ovando-Medina[b,*], Hugo Martínez-Gutiérrez[c], Omar González-Ortega[d]

[a]*Facultad de Agronomía, Universidad Autónoma de San Luis Potosí. Km. 14.5 Carretera San Luis Potosí-Matehuala, Ejido Palma de la Cruz, Soledad de Graciano Sánchez, San Luis Potosí, Apdo. Postal 32,78321, México, Tel. +524441713818; email: paola.diaz@uaslp.mx*
[b]*Ingeniería Química, Coordinación Académica Región Altiplano (COARA), Universidad Autónoma de San Luis Potosí. Carretera a Cedral KM 5+600, San José de las Trojes, Matehuala, San Luis Potosí 78700, México, Tel. +528442245572; email: ovandomedina@yahoo.com.mx (V.M. Ovando-Medina)*
[c]*Centro de Nanociencias y Micro y Nanotecnologías, Instituto Politécnico Nacional (IPN). Luis Enrique Erro S/N, D.F. 07738, México, Tel. +525545664446; email: hamartinez63@hotmail.com*
[d]*Facultad de Ciencias Químicas, Universidad Autónoma de San Luis Potosí. Av. Dr. Manuel Nava No.6, Zona Universitaria, San Luis Potosí, S.L.P. 78210, México, Tel. +524442912743; email: omar.gonzalez@uaslp.mx*

Received 29 July 2018; Accepted 23 February 2019

ABSTRACT

A composite was obtained from α-cellulose coated with magnetite nanoparticles and conducting polypyrrole (PPy). The magnetite nanoparticles were synthesized by the coprecipitation method from $FeCl_2$ and $FeCl_3$ salts. The composite was obtained by pyrrole polymerization in the presence of a mixture of α-cellulose and magnetite nanoparticles. The magnetite nanoparticles and composite were characterized by FTIR and UV/Vis-NIR spectroscopies, scanning electron microscopy (SEM), energy dispersive spectroscopy (EDS), X-ray diffraction (XRD), and thermogravimetric analyses (TGA). XRD analysis demonstrated that magnetite nanoparticles with the typical cubic structures of Fe_3O_4 were obtained. SEM analysis showed that magnetite nanoparticles had irregular morphology with average size of 13 nm, whereas the composite consisted of spherical nanoparticles of PPy coating α-cellulose fibers and magnetite nanoparticles. Batch aqueous adsorption experiments of the reactive black 5 (RB5) dye onto the synthesized material were conducted. The results showed that for the adsorption experiments set to initial pH of 3.0; the maximum adsorption capacity was 62.31 mg of dye g^{-1} of composite, while a value of 21.67 mg of dye g^{-1} of composite was obtained when the initial solution pH was set to 7.0. Adsorption isotherms for the RB5 dye were well described by the Langmuir model. The transient adsorption process of the RB5 dye onto the composite was described by a general three-resistance model; allowing the estimation of the effective diffusivity, D_0, and the adsorption rate coefficient, k_1. For the adsorption experiments with an initial pH value set to 3.0, D_0 was estimated at 4.37×10^{-11} m^2 s^{-1} while k_1 was 7.30×10^{-7} L mg^{-1}.s.

Keywords: Cellulose; Magnetite nanoparticles; Polypyrrole; Dye adsorption; Composite

* Corresponding author.

1. Introduction

According to the 2017 UN World Water Development Report, anthropological activities use water and generate wastewater. Due to the increasing water demand, the quantity of wastewater produced and its overall pollution load are continuously increasing. Over 80% of the wastewater generated worldwide, over 95% in some undeveloped countries, is released to the environment without any treatment. Wastewater is usually discarded into water bodies, diluted or transported downstream, or it infiltrates into aquifers; affecting the quality of freshwater supplies [1].

The textile and leather industries are high water demanding with effluents severely polluted. Therefore wastewater treatment is a global challenge for scientists and governments and at the same time an attractive growth market for industries developing water purification technologies. For example, the market for reverse osmosis membrane elements is currently projected to grow at an above-average rate of 10% annually in the coming three years. In the case of ion exchange resins, future growth is predicted to average 4% per year [2].

In the development of new adsorbent materials; it is important to consider several factors such as raw materials availability, simple synthesis, low cost, reusability and recovery. In this regard different materials have been prepared and studied as natural adsorbents such as coconut fibers waste [3], activated carbon from coconut husk [4], silkworm pupa [5], natural zeolites [6–8], and plants [9,10]. However, it has been observed that composites of two or more natural adsorbents or natural absorbents with synthetic polymers can improve the removal efficiency of different dyes from wastewater. For example, our group recently reported the use of chitosan/zeolite and chitosan/algae composites for fluoride adsorption from aqueous solutions. We observed that at pH 5 the chitosan/zeolite composite had a 1.2-fold increase in fluoride adsorption when compared with the chitosan/algae composite, which showed a higher capacity for fluoride removal at pH 7 [11]. Habiba et al. [12] prepared a composite of chitosan/polyvinyl alcohol/zeolite for the removal of methyl orange and congo red dyes through coagulation and adsorption processes, observing good composite performance in the removal of contaminants.

The preparation of composites with natural adsorbents and synthetic polymers has been of increasing interest since natural absorbents are usually of low cost; provided that they can be originated from wastes (e.g. lignocellulosic materials) or by-products. Moreover, natural adsorbents can be easily combined with small amounts of synthetic polymers; which confer better adsorption properties. Particularly the conducting polymers PPy and polyaniline are of interest due to their good environmental stability, simple synthesis, and high electrical conductivity [13]. On this sense, we reported the preparation of sorghum/PPy composite from sorghum sub-product (cellulosic fibers from stalks) and semiconducting PPy obtained by chemical oxidizing polymerization. This composite was used for the removal of methylene blue dye from aqueous solutions; obtaining a maximum adsorption capacity of 143.5 mg g^{-1} (66.4% more than sorghum fibers alone) [14]. A similar work was reported by Ansari and coworkers [15] who prepared a composite of sawdust from walnut tree and polyaniline; they used it to adsorb methylene blue dye from aqueous solutions at room temperature and pH 9. From their reported Langmuir isotherm data; the maximum adsorption capacity was 8.3 mg g^{-1}. However when using PPy instead of polyaniline; the maximum adsorption capacity increased to 34.3 mg g^{-1} [16]. More recently, we used a composite of α-cellulose/PPy for the removal of the reactive red 120 dye from aqueous solutions. We observed a maximum adsorption capacity of 96.1 mg g^{-1} at acidic pH [17].

Thus, the combination of natural adsorbents and semiconducting polymers increases dye adsorption capacity. However from a practical point of view, adsorbent recovery after dye adsorption is very important since the saturated adsorbent has to be disposed or regenerated for reuse. One option to overcome this recovery problem is the synthesis or preparation of materials with magnetic properties that can be separated using external magnetic fields. Today researchers are paying attention to the synthesis of iron-based magnetic nanoparticles due to their particular structure and properties; which allow their application in several chemical and engineering fields. Compared with their atomic or bulky counterparts; Fe_3O_4 nanoparticles have superior physical and chemical properties due to their mesoscopic effect, small object effect, quantum size effect, surface effect, superparamagnetic character, and non-toxic properties [18]. Some results about the preparation of composites based on PPy and magnetite were reported by Bai et al. [19], who prepared a nanocomposite of water-dispersible graphene-modified magnetic polypyrrole (Fe_3O_4/PPy/RGO) and studied its ability in the methylene blue dye adsorption from aqueous solution. These authors observed a maximum methylene blue adsorption capacity for the composite of 270.3 mg g^{-1} with a Langmuir isotherm. In another work, Ayad et al. [20] reported the synthesis of chitosan/PPy/magnetite nanocomposite for the removal of acid green 25 dye; observing high adsorption capacity when compared with PPy and chitosan alone. The magnetic properties of the composites allowed their recovery at the end of the adsorption process. Asgharinezhad et al. [21] used a composite of multi-walled carbon nanotubes/magnetite nanoparticles/PPy in the co-extraction of acidic, basic, and amphiprotic pollutants (polar and nonpolar).

The objective of the present work was to prepare and characterize a composite of α-cellulose coated with magnetite nanoparticles and the semiconducting PPy as a potential adsorbent of dyes azo type (Fig. 1) from aqueous solutions. A general three-resistance mathematical model was used to describe the adsorption mechanism of the dye onto the surface of the synthesized composite.

2. Experimental setup

2.1. Materials

Pyrrole monomer, reactive black 5 dye, ammonium persulfate, and α-cellulose were purchased from Sigma-Aldrich (>99%) and used as received. $FeCl_2{\cdot}4H_2O$, $FeCl_3{\cdot}6H_2O$, and NaOH were acquired from Jalmek (>97%, Mexico). Deionized water was used in all experiments.

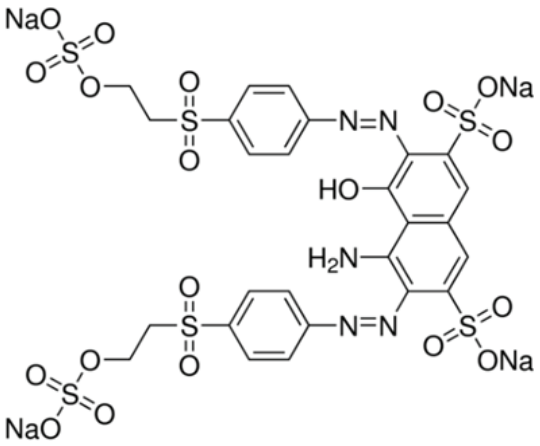

Fig. 1. Chemical structure of the reactive black 5 (RB5) dye.

2.2. Magnetite nanoparticles synthesis

In 100 mL of deionized water; 0.01 mol (1.987 g) of $FeCl_2{\cdot}4H_2O$ and 0.02 mol (5.406 g) of $FeCl_3{\cdot}6H_2O$ were dissolved. This solution was charged to a 250 mL three-neck glass jacketed reactor with mechanical stirring (300 rpm). The mixture was bubbled with argon of ultra-high purity from Infra™ for 1 h to displace dissolved oxygen. In the meantime, 0.08 mol (3.2 g) of NaOH were dissolved in 100 mL of water and purged with argon for 1 h. Afterwards the NaOH solution was transferred to a 100-mL syringe (Hamilton-Gastight), mounted on an addition pump (KdScientific, Cole-Parmer™), and added to the reactor at a rate of 2 mL min^{-1}. After NaOH addition, the reaction was allowed to proceed for 3 h. Subsequently the reaction mixture was poured into a 500-mL beaker, a magnet was placed under the beaker to precipitate the magnetite nanoparticles; the supernatant was discarded. Afterwards, 200 mL of deionized water were added to the magnetite nanoparticles and the precipitation procedure was repeated. This washing process was repeated five times to remove unreacted material. The washed magnetite nanoparticles were dried at 60°C for 24 h.

2.3. α-Cellulose/magnetite nanoparticles/polypyrrole composite preparation

5 g of α-cellulose were dispersed in 50 mL of deionized water in a 125-mL Erlenmeyer flask. In a vial, 1.0 g of magnetite nanoparticles were dispersed in 5 mL of water and immersed into an ultrasonic bath for 2 min to disperse the nanoparticles. Later, the sonicated magnetite nanoparticles dispersion was added to the aqueous α-cellulose dispersion and the mixture was stirred for 5 min. Afterwards, 0.52 g of pyrrole monomer were added and the mixture was stirred for 30 min. Subsequently, 1.77 g of APS was added to start the polymerization process. The reaction was allowed to proceed for 2 h. The resulting composite was precipitated using a magnet placed under the reaction flask and the supernatant was decanted. 50 mL of water were then added, the composite was precipitated again with the magnet, and supernatant was decanted. This washing procedure was repeated five times. The washed composite was dried at 60°C for 24 h.

2.4. Adsorption isotherms and kinetics determination

Batch adsorption experiments were performed at 25°C with initial pH values set to 3.0, 4.0, and 7.0 as follows: 0.1 g of composite were added to a glass vial along with 30 mL of a RB5 dye solution of known concentration in the range from 20 to 200 mg L^{-1}. The pH was adjusted using 0.01 M HCl or NaOH. Vials were continuously stirred using an orbital shaker at constant temperature for 5 d. Adsorbed dye concentration at equilibrium (q_{oe}) was calculated by a mass balance using the initial and final dye concentrations in solution. Concentrations of the RB5 dye throughout the adsorption experiments were determined using a spectrophotometer set to λ = 596 nm (Thermo Scientific, Evolution 220) with a calibration curve constructed with standard solutions in the range from 10 to 300 mg L^{-1}. Adsorption kinetics experiments were run similarly to the equilibrium studies but determining dye solution concentrations at different times.

2.5. Material characterization

The uncoated α-cellulose and the α-cellulose/magnetite nanoparticles/PPy composite were characterized by scanning electron microscopy (JEOL, JSM 7800F). These samples were also analyzed by FTIR with ATR (Cary 630, Agilent) and X-Ray diffraction (XRD) with a PANalytical Empyrean diffractometer using the $Cu_{K\alpha}$ radiation (λ = 1.54056 Å) at 40 kV and 40 mA. The correspondence between the experimental diffraction peaks and the powder diffraction file (PDF) database position was made using the Match! 3 phase identification from powder diffraction software. The specific surface area (A_{BET}) of the composite was determined by N_2 physisorption (Micromeritics, ASAP 2020) using the Brunauer-Emmett-Teller (BET) method. Thermal stability of pure α-cellulose, magnetite, and composite was studied by thermogravimetric analyses (Setaram, Setsys Evolution) using 10 mg of each sample that was heated from 25 to 800°C at a heating rate of 10°C min^{-1}. Point of zero charge (PZC) was determined by titration as follows: in a conical vial the required volume of 0.1 M HCl or NaOH solution was mixed with the volume of a standard 0.1 N NaCl aqueous solution to achieve a final volume of 25 mL with pH in the range from 1.0 to 12.0 (pH_0). After 48 h under magnetic stirring the pH of the resulting solutions was recorded (pH_{0f}). The same procedure of mixture preparation at different pH_0 was repeated but with the addition of 0.1 g of composite and after 48 h of equilibration the pH was measured (pH_f). Data of $\Delta pH = (pH_f - pH_{0f})$ were calculated and plotted as a function of pH_{0f}.

The number of acid and basic active sites was determined by the acid-base titration method. For this 20 mL of 0.1 N HCl (for the basic sites) or NaOH (for the acid sites) aqueous solution were mixed with 0.2 g of adsorbent at 25°C and 70 rpm for 5 d. Afterwards, a 5-mL aliquot was withdrawn and the unreacted HCl or NaOH were titrated with 0.1 N of NaOH or HCl aqueous solutions. Titration was run in triplicate. Active sites concentrations were calculated by the following equations:

$$C_{sa} = \frac{V_i\left(C_i - C_f\right)\times 1000}{m} \quad (1)$$

where C_{sa} represents the active sites concentration in meq g^{-1}, while c_i and c_f are the initial and final concentrations of neutralizing solutions; respectively. V_i is the initial volume of neutralizing solution and m the mass of adsorbent.

Final concentration of neutralizing solution was calculated as follows:

$$c_f = \frac{V_T C_T}{V_m} \quad (2)$$

where C_T is the concentration of titrating solution in eq L^{-1}, V_T is the consumed volume of titrating solution, and V_m is the sample volume of neutralizing solution.

2.6. Mathematical model

In this work, the RB5 dye adsorption mechanism onto the studied composite was described by a general three-resistance model [22] that includes dye transport on the film surrounding the composite particles, dye diffusion in the pores of the composite, and dye adsorption on the surface of the particles. The composite consists of a α-cellulose core, where only diffusion occurs, and a thin shell of magnetite nanoparticles immersed into a PPy matrix, where diffusion and adsorption occur. The equations describing the mathematical model were described elsewhere [17] with the difference that the Langmuir isotherm was used (the model is shown in the supplementary electronic information of this work). The equations of the mathematical model along with the initial and boundary conditions were simultaneously solved by the method of lines [23]. The radial coordinate was discretized using second-order finite differences [24]. Integration in time of discretized equations was performed using the stiff integrator ODE23s from Matlab®. Batch dye uptake data were used to estimate adsorption isotherm parameters. The forward rate coefficient, k_1, was estimated by fitting experimental dye batch uptake data along with the dye effective diffusivity using fminsearch from Matlab®. Both effective diffusivities, D_o and D_p, were considered as being equal for the sake of model simplicity.

3. Results and discussion

3.1. Material characterization

Cellulose is a natural polymer that represents about one-third of plant tissues where it can be restocked by photosynthesis. Cellulose is ordered in micro-fibrils enclosed by hemicellulose and lignin [25]. The molecular structure of cellulose gives some advantages including low density, low extraction cost, recyclability, and biodegradablility [26]. Also due to the presence of the high donor reactivity of the hydroxyl group, which shows tendency to form intra- and inter-molecular hydrogen bonds; a broad chemical variability is present. These characteristics render cellulose as a potential material for composites manufacturing [17]. In this work pyrrole polymerization was enough to wrap-up both cellulose and magnetite, given that intense sonication of the composite in water did not dislodge any component and all the composite was recovered by sedimentation in a magnetic field; therefore we can conclude that cellulose and magnetite are well encapsulated by polypyrrole chains.

Fig. 2 shows the FTIR spectra of α-cellulose, magnetite nanoparticles, PPy, and the α-cellulose/magnetite/PPy composite. It can be seen that the characteristic signals corresponding to cellulose and PPy are present. The assignment of signals to the corresponding chemical group for these two materials is summarized in Table 1. It can also be observed that the spectrum for the composite is similar to that of α-cellulose, with the main difference at 1,562 cm^{-1}; which is related to a mixed C=C and inter-ring C–C vibrations of polypyrrole units. The peak at 1,458 cm^{-1} derives from C–C polypyrrole ring stretching (Ovando-Medina et al. 2014). It is also observed that the cellulose signals corresponding to O–H and C–H stretching (3,300 and 2,900 cm^{-1}, respectively) are less intense in the composite, which is due to the presence of the PPy coating of cellulose fibers. Chemical bonding between cellulose fibers and PPy is desirable since cellulose would be more difficult to

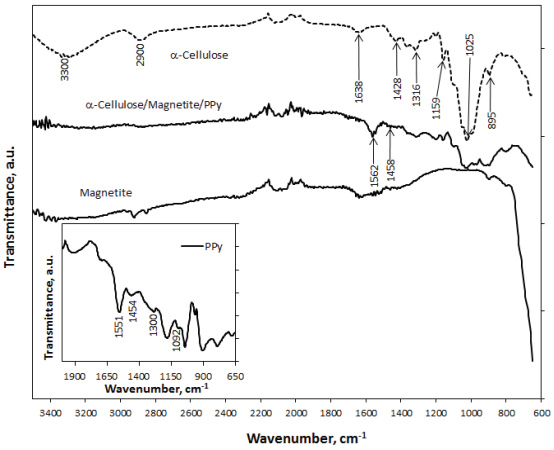

Fig. 2. FTIR spectra of α-cellulose, magnetite, PPy (inset), and the prepared composite.

Table 1
FTIR assignments of the main signals of PPy and cellulose

Signal, cm^{-1}	Chemical group
IR signals corresponding to PPy	
1,551	C=C backbone stretching
1,454	C–C ring stretching
1,300	C–H in-plane
1,092	C–N stretching vibrations
Main signals corresponding to cellulose	
895	Stretching COC at b-glycosidic linkage
1,046	Stretching CO at C6
1,161	Stretching COC at b-glycosidic linkage
1,323	Bending CH_2 (wagging) at C–6
1,417	Bending CH_2 (sym) at C–6
1,638	–O- tensile vibration neighboring hydrogen atoms
2,900	Stretching C–H
3,300	Stretching O–H (hydrogen bonded)

separate from the PPy layer. It would be expected that this bonding would take place through –OH groups of cellulose and the –NH groups of polypyrrole rings. From Fig. 2 it can be observed that bands at 1,551 and 1,454 cm^{-1} for pure polypyrrole (inset in Fig. 2) are shifted to 1,562 and 1,458 cm^{-1} for the composite. The observed shift of these bands may be due to chemical bonding between NH– in the pyrrole ring and the –OH groups of cellulose [27,28]. FTIR signals corresponding to magnetite are usually observed between 500 and 600 cm^{-1}, therefore XRD analyzes were performed to magnetite and the composite.

Figs. 3(a) and (b) show the X-ray diffractograms of magnetite alone and the α-cellulose/magnetite/PPy composite. The positions of the diffraction peaks associated with the cubic crystal structures of Fe_3O_4 (magnetite) from the 190629 PDF card are shown as well. As can be seen (Fig. 3(a)) the main peaks presented in the diffractograms are due to diffraction from the (220), (311), (222), (400), (422), (511), (440), (531), (620), and (533) planes; which are supposed to represent the typical Fe_3O_4 structure. The X-ray diffraction analysis corroborates that the sample is composed of Fe_3O_4 since there is a complete correspondence between the diffraction peaks and the database positions. The observed (strong and sharp) diffraction peaks suggest that the layers are highly crystalline. On the other hand the diffractogram corresponding to the composite (Fig. 3(b)) only shows three broad peaks, which are due to the amorphous structure of the PPy coating the cellulose and magnetite nanoparticles. In the XRD analysis only one peak is usually observed for PPy; depending on the synthesis process this peak is observed between 22° and 25° of 2θ [29]. In our case, the other signals can be due to the crystalline part of cellulose (15°, 22.5°, and 35° of 2θ) [30]; the XRD peaks corresponding to magnetite nanoparticles in the composite are almost imperceptible given the PPy coating.

Thermogravimetric analysis was carried out to investigate the thermal properties of the α-cellulose/magnetite/PPy composite; the results are shown in Fig. 4. As can be seen in this Fig. 4, magnetite nanoparticles are highly stable due to their inorganic nature; only 4% of weight loss was observed. α-cellulose showed a decomposition temperature around 260°C, nonetheless in the composite the onset of decomposition decreased to 200°C; which corresponds to PPy degradation. The decomposition rate was slower for the composite, which can be ascribed to the presence of magnetite nanoparticles that reduce PPy and α-cellulose chains mobility. In addition the weight loss of composite after 550°C was 88.7% (11.3% of inorganic materials composed of magnetite nanoparticles and ashes from cellulose and PPy), whereas for α-cellulose the weight loss was close to 96.5% (3.5% of ashes); this implies that the composite contains 7.8% of magnetite nanoparticles even though 20% of magnetite was used in the preparation. We have calculated from PPy conversion and this magnetite amount that approximately 23% of PPy and magnetite are coating the α-cellulose fibers.

Fig. 5 shows SEM images of uncoated α-cellulose (Fig. 5(a)), magnetite nanoparticles (Fig. 5(b)), and the α-cellulose/magnetite/PPy composite at two different magnifications (Figs. 5(c) and (d)). It can be observed that uncoated cellulose shows the typical surface of fibers reported in the literature with relatively homogeneous morphology compared to that observed for the as prepared composite (Fig. 5(c)). Magnetite nanoparticles presented irregular morphology with small sizes ranging between 7 and 18 nm (Fig. 5(b)). Fig. 6 shows the particle size distribution of the synthesized magnetite nanoparticles. It can be observed that narrow PSD was obtained through this process with a number-average particle size (Dn) of 13 nm and polydispersity index in size of 1.1; demonstrating the monomodal PSD shape. Sizes here observed are relatively small taking into account that the synthesis was made without any

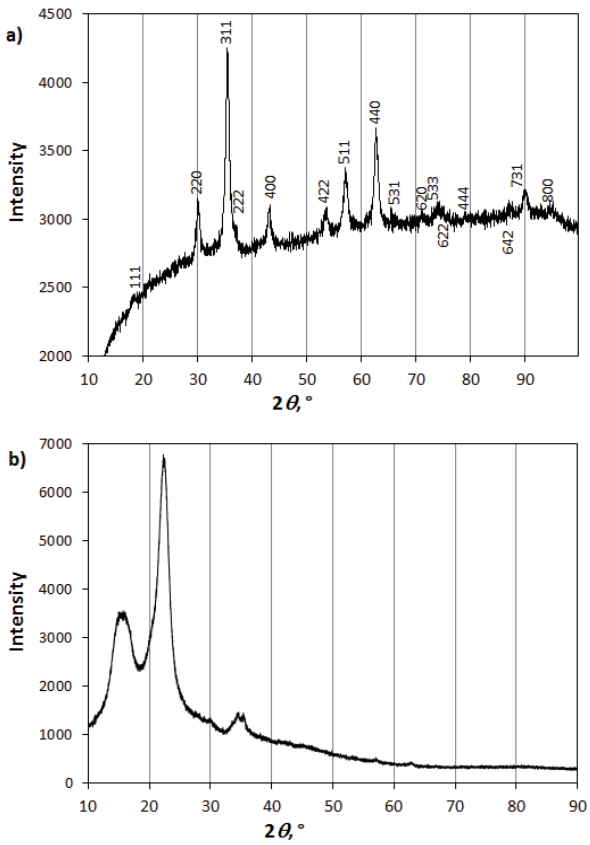

Fig. 3. XRD patterns for magnetite (a) and the α-cellulose/magnetite/PPy nanocomposite (b).

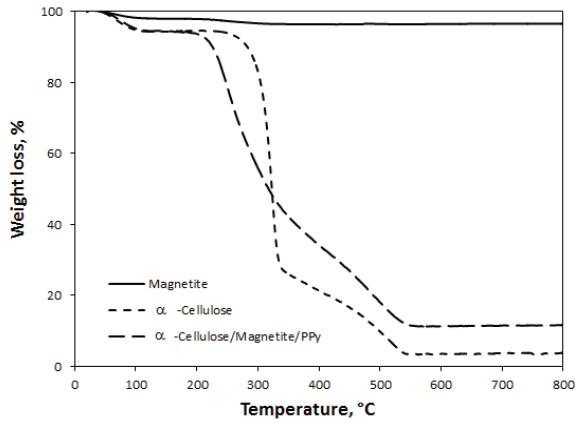

Fig. 4. TGA analyzes of composite, magnetite nanoparticles, and α-cellulose.

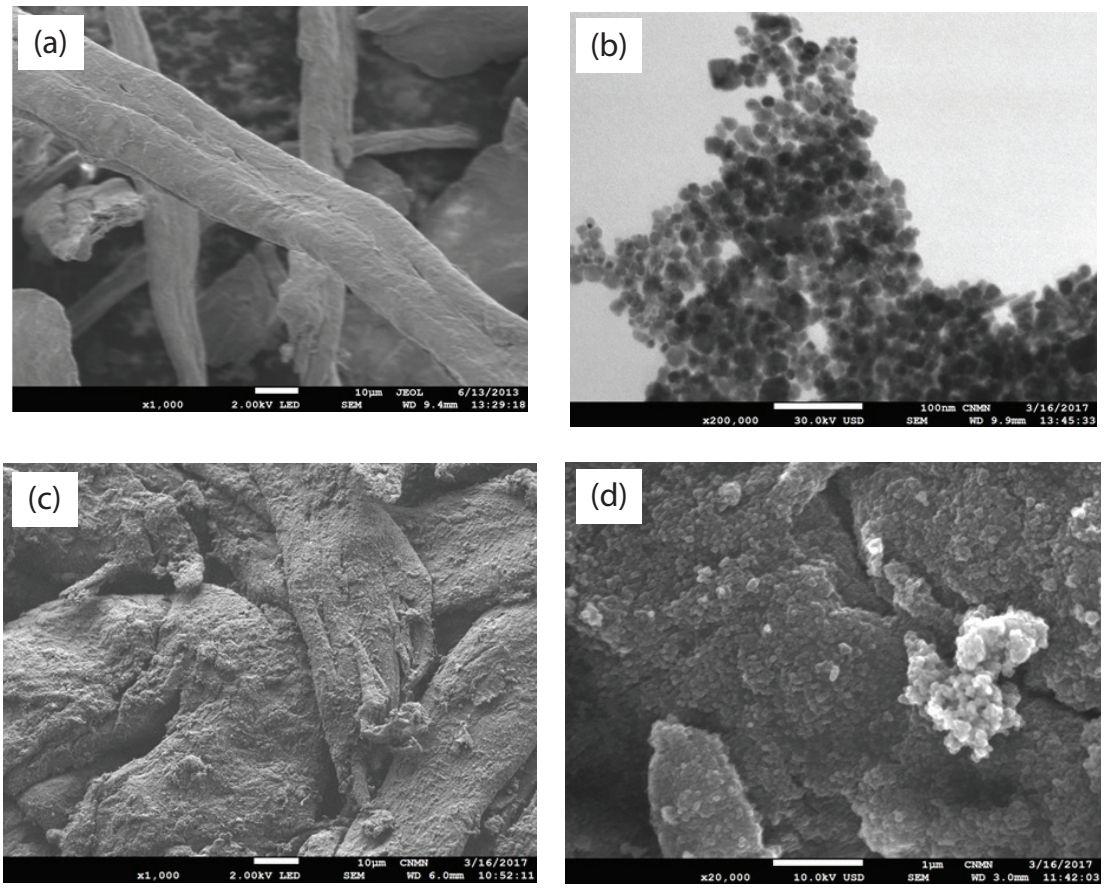

Fig. 5. SEM images of α-cellulose (a), synthesized magnetite nanoparticles in STEM mode (b), and SEM of the compos ite of α-cellulose/magnetite/PPy × 1,000 (c) and × 20,000 (d).

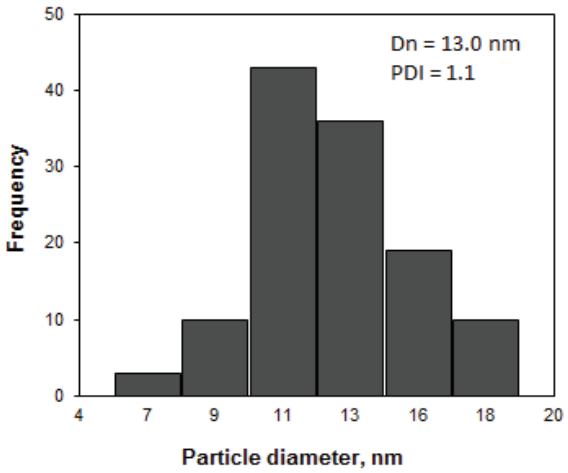

Fig. 6. PSD of magnetite nanoparticles.

surfactant or template and are similar to those observed by Mascolo et al. [31] using different bases for magnetite precipitation. For example Goya et al. [32] reported magnetite nanoparticles sizes in the range from 5 to 150 nm when precipitating hematite particles by forced hydrolysis of a $FeCl_3$ solution at 100°C for 2 d and further reduction under 1 atm of hydrogen at 360°C for 3.5 h. Sun and Zeng [33] prepared magnetite nanoparticles by high-temperature solution-phase reaction of Fe(III) acetylacetonate in phenyl ether with alcohol, oleic acid, and oleylamine; obtaining sizes between 20 and 30 nm. From Fig. 5(c), it can be seen that the α-cellulose fibers and magnetite nanoparticles are coated by PPy; showing some PPy agglomerates. PPy consisted of well-defined monodispersed spherical particles (Fig. 5(d)) with average diameter of 70 nm providing a large available surface area for chemical and physical interactions and electronic conductions. This PPy diameter is smaller than the observed value of 90 nm for PPy over pure α-cellulose previously reported [17], which demonstrates that magnetite nanoparticles affected the PPy nanoparticles size. The PPy morphology was typical of pyrrole polymerization on hydrophilic surfaces [34,35].

Fig. 7(a) shows an SEM image of the composite with contrast where two different materials can be observed; therefore EDS analyses were performed to the different zones marked with arrows in Fig. 7(a) (Zones A and B). Fig. 7(b) and (c) are the corresponding EDS spectra of these two zones. It can be seen that high C and O intensities are present in Fig. 7(b) and a small amount of sulfur from traces of the APS used in the pyrrole polymerization. Almost no Fe was detected in zone A. EDS spectrum of zone B shows high concentrations of Fe and O (Fig. 7(c)). Thus, we can conclude that the small brilliant zones in the composite (Fig. 7(a)) mainly correspond to uncoated agglomerates of

magnetite nanoparticles. Compositions in weight% and atomic % from the EDS analyses are shown in Table 2. From atomic percentages of Fe and O in this Table, we can calculate an O/Fe atomic ratio of 1.60; this value is 20% higher than the 1.33 expected for Fe_3O_4. The difference can be due to oxygen from –OH groups of the cellulose and the inherent analysis error.

3.2. Kinetics and batch adsorption experiments

The surface adsorption properties and the affinity between adsorbate and the adsorbent are described by the equilibrium adsorption isotherm. Equilibrium is reached when the concentration of sorbate in the solution is in dynamic balance with the concentration of the sorbate at the adsorbent interface. In this work, the experimental data of adsorption capacity in aqueous solutions were fitted by the Langmuir and Freundlich models:

Langmuir model:

$$Q_e = Q_m C_e / \left(1/K_L + C_e\right) \tag{3}$$

Freundlich model:

$$Q_e = K_F \left(C_e\right)^n \tag{4}$$

where Q_e is the adsorption capacity at the equilibrium concentration C_e, K_L is a Langmuir constant (related to the affinity of binding sites), Q_m is the maximum adsorption capacity, K_F is the Freundlich constant, and n is the surface heterogeneity constant in the Freundlich model.

The constants for these isotherms were evaluated by a least-squares method using an optimization algorithm. The average absolute deviation percentage was calculated as follows:

$$\%D = \left(\frac{1}{N}\sum_{i=1}^{N}\left|\frac{Q_{\exp} - Q_{\text{pred}}}{Q_{\exp}}\right|\right) \times 100\% \tag{5}$$

where N represents the number of data, $Q_{\exp}$ is the experimental adsorption capacity, and Q_{pred} is the predicted adsorption capacity. The Freundlich and Langmuir parameters corresponding to adsorption experiments onto the α-cellulose/magnetite/PPy composite at different pH values are presented in Table 3. As can be seen from this table, the Langmuir model fits best the experimental data. In other words according to the Langmuir model, adsorption of the RB5 dye is mainly associated to monolayer sorption rather than adsorption on a surface with heterogeneous energy distribution.

Fig. 8(a) shows the adsorption isotherms (based on the total mass of composite) of the RB5 dye onto the α-cellulose/magnetite/PPy composite at pH 3.0, 4.0, and 7.0.

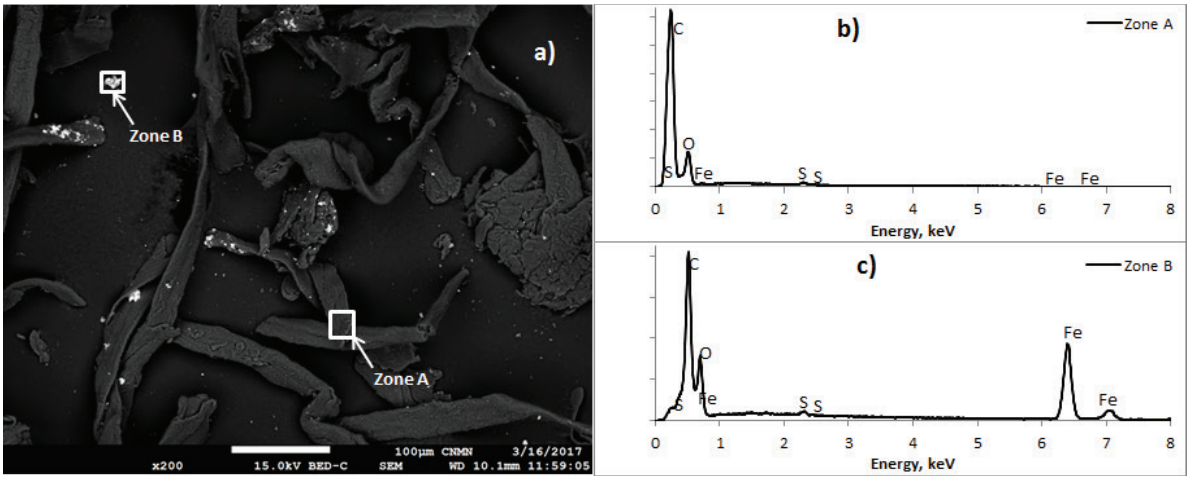

Fig. 7. SEM image of the composite with contrast (a), EDS spectra of zones A (b) and B (c).

Table 2
Compositions in weight and atomic percentages determined from EDS analyzes of zones A and B shown in Fig. 7(a)

Element	Zone A			Zone B		
	Weight (%)	Atomic (%)	Error (%)	Weight (%)	Atomic (%)	Error (%)
C_K	69.63	75.52	4.04	–	–	–
O_K	29.8	24.26	9.51	31.41	61.52	5.12
S_K	0.45	0.18	7.16	–	–	–
Fe_K	0.12	0.03	58.26	68.59	38.48	2.86

It can be seen from Table 3 and Fig. 8(a), that the maximum adsorption capacity decreases with the pH value of the dye solution. In other words, the dye adsorption energy at acidic pH is lower than that needed at a higher pH. This behavior can be explained with the point of zero charge (PZC) of the composite that is shown in Fig. 8(b). The PZC was determined as 1.2, this implies that in an aqueous dispersion of the composite with pH set to 1.2; the sum of + and – charges is zero at the surface of the composite. At higher pH values the surface is predominantly negative in character. It is noticeable that the composite showed an almost neutral charge in the pH interval from 1.2 to 3.2; if the pH value increases beyond 3.2 the surface charge becomes highly negative until a limit is reached at pH close to 9.0. The RB5 dye is an anionic molecule upon water dissociation as shown in Fig. 1; therefore favorable electrostatic interactions between the dye and the surface of composite at pH below 3.2 are expected, where the zero point charge is almost reached. It is well known that other physical adsorption mechanisms can occur.

Table 3
Estimated parameters of Langmuir and Freundlich models calculated from experimental equilibrium batch adsorption data at different pH

Langmuir model				
pH	Q_m	K_L	R^2	%D
3	62.31	0.048	0.96	11.8
4	36.19	0.059	0.88	13.2
7	21.67	0.050	0.98	2.20
Freundlich model				
pH	K_F	n	R^2	%D
3	9.35	0.379	0.81	28.1
4	6.87	0.324	0.97	3.50
7	4.04	0.324	0.93	7.50

Note: Q_m in mg g^{-1}; K_L in mg^{-1} L^{-1}; K_F in mg^{1-n} L^n g^{-1}.

Fig. 9 shows different proposed adsorption mechanisms of the RB5 dye onto the α-cellulose/magnetite/polypyrrole composite. The attachment through π–π* (bonding-antibonding) interactions between the electrons of the aromatic rings of the dye molecules and the electrons from pyrrole rings is considered. High affinity of the dye for the composite surface can also result from hydrogen bond formation, which can be created between nitrogen from the pyrrole ring and nitrogen from the $–NH_2$ group of the dye as well as oxygen of uncoated magnetite with the $–NH_2$ group of the dye. Moreover, interactions between the oxygen atom from magnetite and the oxygen atom from hydroxyl groups or the nitrogen atom from the azo group of the dye through water molecules can exist. In order to differentiate

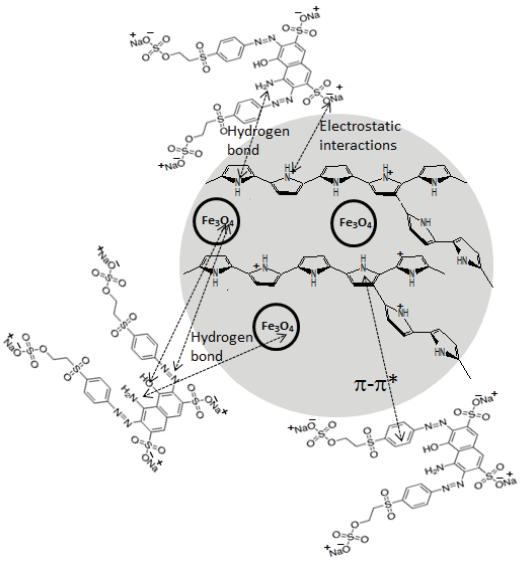

Fig. 9. Proposed interactions between the RB5 dye and the PPy coating from the studied composite (Modified from Wawrzkiewicz and Hubicki [36]).

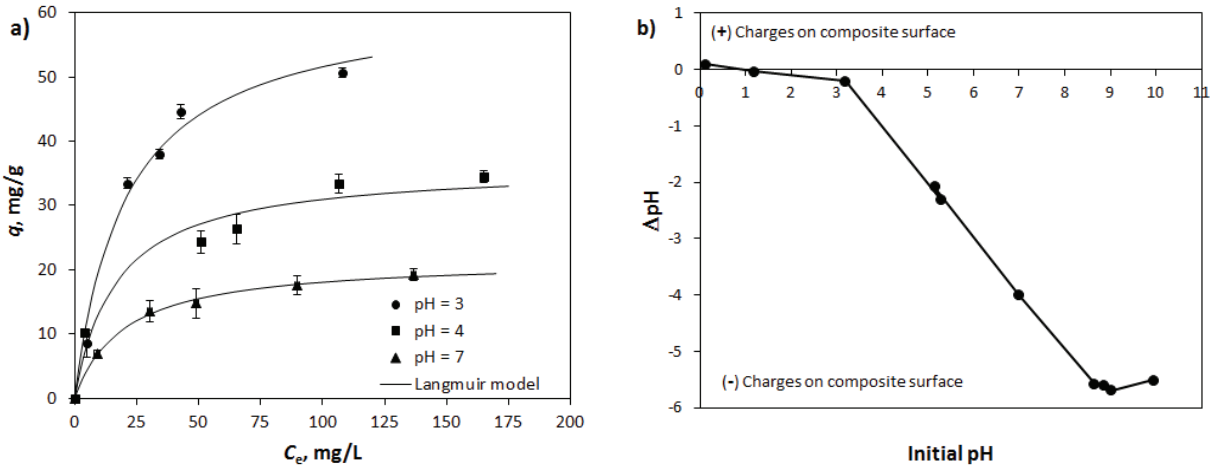

Fig. 8. (a) Isotherms of RB5 dye adsorption onto α-cellulose/magnetite/PPy composite at different pH values. (b) Point of zero charge curve for the synthesized composite.

electrostatic interactions from the others, we determined the active sites number through a titration method obtaining values of 1.97 meq g^{-1} of composite for the acid sites and 0.39 meq g^{-1} of composite for the basic sites. The maximum adsorption reached at pH = 3.0 was 62.31 mg g^{-1} of composite, which corresponds to 0.25 meq g^{-1} of composite. This value is 7.8 times smaller than the one determined for the acid active sites, which implies that not all the sites are available for adsorption; however, it is difficult to exactly discriminate the adsorption mechanisms. It is worth mentioning that the composite was recovered from the aqueous solutions using an external magnet; contributing to the simple application of the proposed material.

Fig. 10(a) shows the hysteresis curve obtained from the N_2 adsorption-desorption analysis. It can be seen that the adsorbed N_2 amount was very low at any value of relative pressure. The hysteresis phenomenon can be associated with the capillary condensation in mesoporous structures. Different forms of the hysteresis loop are caused by different types of adsorbent and sorption experimental conditions such as temperature and pressure [37]. According to the IUPAC, the curve shown in Fig. 10(a) corresponds to H3 hysteresis loop type and no micropores were observed since there is no tendency to form a plateau at low relative pressures [38]. The experimental BET area of α-cellulose was determined as 0.45 m^2 g^{-1}; while the corresponding value for the composite was 12.19 m^2 g^{-1}, which can be ascribed to the deposition of PPy nanoparticles coating α-cellulose fibers; then, the porosity generated in the composite is mainly due to PPy interparticle and intercluster spaces (Fig. 10(b)).

The experimental and simulated adsorption kinetics data for the RB5 dye at a pH value set to 3.0 using 0.1 g of composite and 100 mg L^{-1} of initial dye concentration are shown in Fig. 11. The forward rate coefficient, k_1, was estimated by fitting the three-resistance mathematical model to the experimental dye batch uptake data along with the dye effective diffusivity using an initial dye concentration of 100 mg L^{-1}. Afterwards, these optimized parameters were used to simulate the data for the two condition sets shown below. Table S1 of supplementary electronic information shows the values for all the non-fitted parameters used in the simulations. The value used for the apparent density (ρ_p) of the adsorbent particles was taken as 1.46 g mL^{-1} since cellulose density values are in the range from 1.3 to 1.5 g mL^{-1} [27]. Shell density (ρ_o) was fixed to 1.45 g mL^{-1}. Core porosity for cellulose powder (ε_i) was reported by Bhimte and Tayade [39], while shell porosity for PPy and magnetite film (ε_o) was fixed to 0.35. From Fig. 11, it can be seen that the mathematical model shows a good representation of the experimental adsorption kinetic data. The estimated values for k_1 and D_o where 7.30×10^{-7} L mg·s^{-1} and 4.37×10^{-11} m^2 s^{-1}, respectively.

It is difficult to compare the adsorption rate coefficient with information in the literature since most of the times simplified models are used to describe adsorption of dyes [40–42] such as the pseudo-first order and the pseudo-second order models. Furthermore, these models are sensitive to the initial concentration of dye and multiple fittings need to be performed; moreover, these models are based on the dye concentration on the adsorbent discarding important resistances to mass transfer. To assess the predictive capacity of the mathematical model, two predictions were run. For the first run the mass of composite (W_A) and the initial

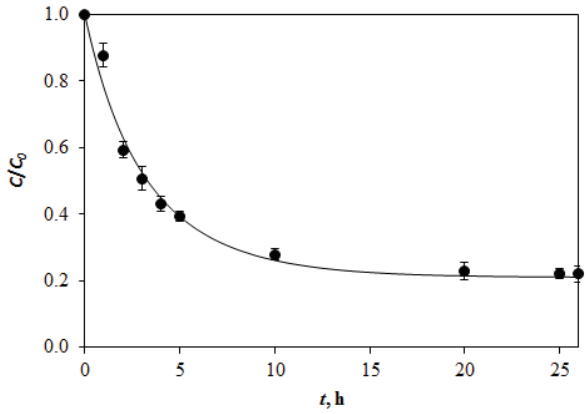

Fig. 11. Kinetics adsorption of the RB5 dye (dimensionless dye concentrations in the bulk liquid, c) at initial dye concentration C_A = 100 mg L^{-1} and using 0.1 g of composite.

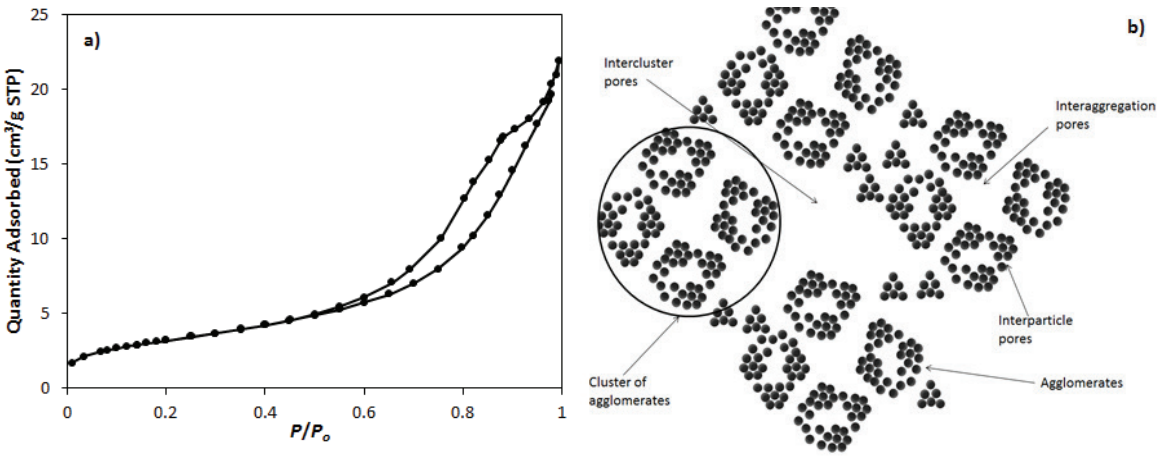

Fig. 10. (a) Hysteresis curve of N_2 adsorption-desorption for the synthesized composite and (b) proposed structural elements and pore types of PPy nanoparticles coating cellulose and magnetite in the composite.

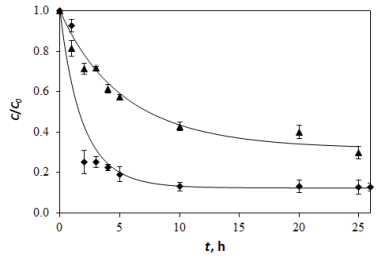

Fig. 12. Kinetics adsorption of the RB5 dye (dimensionless dye concentrations in the bulk liquid, c) at initial dye concentration C_A = 50 mg L^{-1} and 0.1 g of composite (triangles); and C_A = 100 mg L^{-1} and 0.15 g of composite (diamonds).

dye concentration (C_A) were set to 0.15 g and 100 mg L^{-1} while for the second run C_A and W_A were set to 50 mg L^{-1} and 0.1 g, respectively. Fig. 12 shows both predictions along with the experimental results of batch uptake experiments. It can be seen that the mathematical model performs a fair prediction of the batch dye adsorption behavior using the studied composite.

As shown in the supplementary information, adsorption-desorption cycles were performed to determine the stability and recoverability after use of the composite. It can be seen from Fig. S1 of the supplementary information that for two adsorption cycles, dye removal percentages remain almost constant at 74%, 56%, and 72% for initial dye concentrations of 50, 100, and 150 mg L^{-1}; respectively, demonstrating the stability of the studied composite.

4. Conclusions

A composite of α-cellulose/magnetite nanoparticles/PPy was prepared and characterized. It was observed that magnetite presented the typical cubic crystal structure corresponding to Fe_3O_4, irregular morphology with average size of 13.0 nm, and monomodal PSD. Also, the composite consisted of PPy nanoparticles with approximate size of 70 nm coating α-cellulose fibers and magnetite nanoparticles. This composite showed a low BET area (11.42 m^2 g^{-1}), which was ascribed to the presence of mosopores derived from interparticle and intercluster spaces of the PPy particles. The composite showed potential as adsorbent of the RB5 dye from aqueous solutions at acidic pH, through the adsorption derived from electrostatic interactions between the dye and the positively charged surface of the composite at this pH value. The adsorption process was defined by the Langmuir isotherm with a maximum adsorption capacity of 62.31 mg of RB5 dye g^{-1} of composite. Kinetics of RB5 dye adsorption was well described with the three-resistance mathematical model obtaining, for the experiments set to initial pH of 3.0, a D_o of 4.37×10^{-11} m^2 s^{-1} and k_1 of 7.30×10^{-7} L mg·s^{-1}.

Acknowledgements

Camerina J. Guzmán Álvarez acknowledges a scholarship from CONACYT for MSc studies through the Grant PDCPN-2015-384, #25941. Author Paola E. Díaz-Flores acknowledges to Elizabeth Diane Isaacs Páez from IPICYT-México by her help in BET determinations. This work was supported by CONACYT through Grant PDCPN-2015-384.

Author contributions

Víctor M. Ovando-Medina conceived the idea, designed the experiments, and wrote the manuscript; Paola E. Díaz-Flores designed and discussed the adsorption experiments, Camerina J. Guzmán-Álvarez performed the experiments and discussed part of the results; Hugo Martínez-Gutiérrez performed the SEM analysis; Omar González-Ortega implemented and discussed the mathematical model.

Conflict of interest

Authors declare no conflict of interest.

References

[1] The United Nations World Water Development Report 2017 (2017). Wastewater: The Untapped Resource. The United Nations World Water Development Report, Paris. Available at: http://unesdoc.unesco.org/images/0024/002475/247552e.pdf (Accessed 21 July 2017).
[2] Water and wastewater International: case study: textile dyeing without effluent. Available at: http://www.waterworld.com/articles/wwi/2017/02/case-study-textile-dyeing-without-effluent.html, 2017 (Accessed 02 August 2017).
[3] B.H. Hameed, D.K. Mahmoud, A.L. Ahmad, Equilibrium modeling and kinetic studies on the adsorption of basic dye by a low-cost adsorbent: coconut (Cocos nucifera) bunch waste, J. Hazard. Mater., 158 (2008) 65–72.
[4] I.A.W. Tan, A.L. Ahmad, B.H. Hameed, Adsorption of basic dye on high-surface-area activated carbon prepared from coconut husk: equilibrium, kinetic and thermodynamic studies, J. Hazard. Mater., 154 (2008) 337–346.
[5] B. Noroozi, G.A. Sorial, H. Bahrami, M. Arami, Equilibrium and kinetic adsorption study of a cationic dye by a natural adsorbent—Silkworm pupa, J. Hazard. Mater., 139 (2007) 167–174.
[6] K.Y. Hor, J.M.C. Chee, M.N. Chong, B. Jin, C. Saint, P.E. Poh, R. Aryal, Evaluation of physicochemical methods in enhancing the adsorption performance of natural zeolite as low-cost adsorbent of methylene blue dye from wastewater, J. Cleaner Prod., 118 (2016) 197–209.
[7] O.A. Saputra, M.D. Prameswari, V.T.D. Kinanti, O.D. Mayasari, Y.D. Sutarni, K. Apriany, W.W. Lestari, Preparation, characterization and methylene blue dye adsorption ability of acid activated-natural zeolite, IOP Conf. Ser.: Mater. Sci. Eng., 172 (2017) 012039.
[8] I. Humelnicu, A. Băiceanu, M.-E. Ignat, V. Dulman, The removal of Basic Blue 41 textile dye from aqueous solution by adsorption onto natural zeolitic tuff: kinetics and thermodynamics, Process Saf. Environ. Prot., 105 (2017) 274–287.
[9] R. Aziam, M. Chiban, E. Eddaoudi, A. Soudani, M. Zerbet, F. Sinan, Factors controlling the adsorption of acid blue 113 dye from aqueous solution by dried C. edulis plant as natural adsorbent, Arabian J. Geosci., 9 (2016) 659.
[10] M. Shirzad-Siboni, A. Khataee, F. Vafaei, S.W. Joo, Comparative removal of two textile dyes from aqueous solution by adsorption onto marine-source waste shell: kinetic and isotherm studies, Korean J. Chem. Eng., 31 (2014) 1451.
[11] A. Pérez-Escobedo, P.E. Díaz-Flores, J.R. Rangel-Méndez, F.J. Cerino-Cordova, V.M. Ovando-Medina, J.A. Alcalá-Jáuregui, Fluoride adsorption capacity of composites based on chitosan-zeolite-algae, Rev. Mex. Ing. Chím., 15 (2016) 139–147.
[12] U. Habiba, T.A. Siddique, T.C. Joo, A. Salleh, B.C. Ang, A.M. Afifi, Synthesis of chitosan/polyvinyl alcohol/zeolite composite for removal of methyl orange, Congo red and chromium(VI) by flocculation/adsorption, Carbohydr. Polym., 157 (2017) 1568–1576.

[13] H. Wang, T. Lin, A. Kaynak, Polypyrrole nanoparticles and dye absorption properties, Synth. Met., 151 (2005) 136–140.
[14] V.M. Ovando-Medina, P.E. Díaz-Flores,, H. Martínez-Gutiérrez, L.A. Moreno-Ruiz, Antonio-I.D. Carmona, M. Hernández-Ordoñez, Composite of cellulosic agricultural waste coated with semiconducting polypyrrole as potential dye remover, Polym. Compos., 35 (2014) 186–193.
[15] M. Banimahd-Keivani, K. Zare, H. Aghaie, R. Ansari, Removal of methylene blue dye by application of polyaniline nano composite from aqueous solutions, J. Phys. Theor. Chem. IAU Iran, 6 (2009) 63–70.
[16] R. Ansari, Z. Mosayebzadeh, Removal of basic dye methylene blue from aqueous solutions using sawdust and sawdust coated with polypyrrole, J. Iran. Chem. Soc., 7 (2010) 33–35.
[17] V.M. Ovando-Medina, J. Vizcaíno-Mercado, O. González-Ortega, J.A. Rodríguez de la Garza, H. Martínez-Gutiérrez, Synthesis of α-cellulose/polypyrrole composite for the removal of reactive red dye from aqueous solution: kinetics and equilibrium modeling, Polym. Compos., 36 (2015) 312–321.
[18] A.R. Bagheri, M. Ghaedi, A. Asfaram, A.A. Bazrafshan, R. Jannesar, Comparative study on ultrasonic assisted adsorption of dyes from single system onto Fe_3O_4 magnetite nanoparticles loaded on activated carbon: experimental design methodology, Ultrason. Sonochem., 34 (2017) 294–304.
[19] L. Bai, Z. Li, Y. Zhang, T. Wang, R. Lu, W. Zhou, H. Gao, S. Zhang, Synthesis of water-dispersible graphene-modified magnetic polypyrrole nanocomposite and its ability to efficiently adsorb methylene blue from aqueous solution, Chem. Eng. J., 279 (2015) 757–766.
[20] M. Ayad, N. Salahuddin, A. Fayed, B.P. Bastakoti, N. Suzuki, Y. Yamauchi, Chemical design of a smart chitosan–polypyrrole–magnetite nanocomposite toward efficient water treatment, Phys. Chem. Chem. Phys., 16 (2014) 21812–21819.
[21] A.A. Asgharinezhad, H. Ebrahimzadeh, Coextraction of acidic, basic and amphiprotic pollutants using multiwalled carbon nanotubes/magnetite nanoparticles@polypyrrole composite, J. Chromatogr. A, 1412 (2015) 1–11.
[22] R.M. Montesinos, R. Guzmán, A. Tejeda-Mansir, Simulation of stirred tank affinity processes applied to separation of proteins, Int. J. Bio-Chromatogr., 6 (2001) 231–243.
[23] S. Chapra, R. Canale, Numerical methods for engineers, McGraw-Hill, New York, 1983.
[24] C.J. Geankoplis, Transport processes and unit operations, Allyn and Bacon, Boston, 1983.
[25] J.I. Morán, V.A. Alvarez, V.P. Cyras, A. Vázquez, Extraction of cellulose and preparation of nanocellulose from sisal fibers, Cellulose, 15 (2008) 149–159.
[26] X. Li, L.G. Tabil, S. Panigrahi, Chemical treatments of natural fiber for use in natural fiber-reinforced composites: a review, J. Polym. Environ., 15 (2007) 25–33.
[27] J.H. Johnston, F.M. Kelly, J. Moraes, T. Borrmann, D. Flynn, Conducting polymer composites with cellulose and protein fibres, Curr. Appl. Phys., 6 (2006) 587–590.
[28] D. Müller, C.R. Rambo, D.O.S. Recouvreux, L.M. Porto, G.M.O. Barra, Chemical *in situ* polymerization of polypyrrole on bacterial cellulose nanofibers, Synth. Met., 161 (2011) 106–111.
[29] N. Su, H.B. Li, S.J Yuan, S.P. Yi, E.Q. Yin, Synthesis and characterization of polypyrrole doped with anionic spherical polyelectrolyte brushes, Express Polym. Lett., 6 (2012) 697–705.
[30] A. Kumar, Y.S. Negi, V. Choudhary, N.K. Bhardwaj, Characterization of cellulose nanocrystals produced by acid-hydrolysis from sugarcane bagasse as agro-waste, J. Mat. Phys. Chem., 2 (2014) 1–8.
[31] M.C. Mascolo, Y. Pei, T.A. Ring, Room temperature co-precipitation synthesis of magnetite nanoparticles in a large pH window with different bases, Materials, 6 (2013) 5549–5567.
[32] G.F. Goya, T.S. Berquó, F.C. Fonseca, Static and dynamic magnetic properties of spherical magnetite nanoparticles, J. Appl. Phys., 94 (2003) 3520–3528.
[33] S. Sun, H. Zeng, Size-controlled synthesis of magnetite nanoparticles, J. Am. Chem. Soc., 124 (2002) 8204–8205.
[34] J.H. Johnston, J. Moraes, T. Borrmann, Conducting polymers on paper fibres, Synth. Met., 153 (2005) 65–68.
[35] G. Nyström, A. Mihranyan, A. Razaq, T. Lindström, L. Nyholm, M. Strømme, A Nanocellulose polypyrrole composite based on microfibrillated cellulose from wood, J. Phys. Chem. B, 114 (2010) 4178–4182.
[36] M. Wawrzkiewicz, Z. Hubicki, In: A. Kilislioglu, Ion Exchange - Studies and Applications, InTech, pp. 37–72.
[37] L. Qi, X. Tang, Z. Wang, X. Peng, Pore characterization of different types of coal from coal and gas outburst disaster sites using low temperature nitrogen adsorption approach, Int. J. Mining Sci. Tech., 27 (2017) 371–377.
[38] L.F. Ballesteros, J.A. Teixeira, S.I. Mussatto, Chemical, functional, and structural properties of spent coffee grounds and coffee silverskin, Food Bioprocess Technol., 7 (2014) 3493–3503.
[39] N.A. Bhimte, P.T. Tayade, Evaluation of microcrystalline cellulose prepared from sisal fibers as a tablet excipient: a technical note, AAPS Pharm. Sci. Tech., 8 (2007) E56–E62.
[40] Z. Eren, F.N. Acar, Adsorption of reactive black 5 from an aqueous solution: equilibrium and kinetic studies, Desalination, 194 (2006) 1–10.
[41] T.K. Saha, N.C. Bhoumik, S. Karmaker, M.G. Ahmed, H. Ichikawa, Y. Fukumori, Adsorption characteristics of reactive black 5 from aqueous solution onto chitosan, CLEAN–Soil, Air, Water, 39 (2011) 984–993.
[42] D. Karadag, M. Turan, E. Akgul, S. Tok, A. Faki, Adsorption equilibrium and kinetics of reactive black 5 and reactive red 239 in aqueous solution onto surfactant-modified zeolite, J. Chem. Eng. Data, 52 (2007) 1615–1620.
[43] L. Donnaperna, L. Duclaux, R. Gadiou, Adsorption of Remazol Black B Dye on Activated Carbon Felt, Carbon – Sci. Technol., 1 (2008) 66–71.

Supplementary information

1. Adsorption-desorption cycles

Two cyclic experiments of adsorption-desorption were made to determine the recoverability and stability of the composite. Batch adsorption test were made as described in the methodology section of paper at 50, 100 and 150 mg L^{-1} of initial dye concentration at pH of 3.0. Desorption test were achieved pouring 0.1 g of dye saturated composite (previously used for adsorption experiments) in 30 mL of distilled water, and adjusting the pH at 9.0 at 70 rpm of stirring rate through 6 d. Afterwards, composite was recovered and dried to be used again in a second adsorption experiment. The percentages of adsorbed dye were calculated from a mass balance and the results are shown in Fig. S1.

2. Dye uptake model

In this work, the reactive black 5 dye batch adsorption kinetics using the proposed composite is presented. A mathematical model was used to fit the experimental data to determine the values of selected parameters. The model is a general three-resistance model that includes the transport on the film that surrounds the composite particles, diffusion inside the particles and adsorption on the surface of the particles. The proposed composite is visualized as a core-shell particle with cellulose as core and magnetite-containing polypyrrol as shell. The studied dye is allowed to diffuse in both the core and the shell while adsorption only occurs on the shell.

The batch adsorption process consists of a bulk liquid and a solid (composite). Since the bulk liquid is considered well-stirred such that a macroscopic balance on the dye can be performed, this results in Eq. (1) where the movement of dye in the boundary layer produces a temporal change in dye concentration in the liquid outside the composite.

$$V_L \frac{dC}{dt} = -3\frac{W_A k_f}{\rho_p R_o}\left(C - C_o\big|_{R=R_o}\right) \tag{1}$$

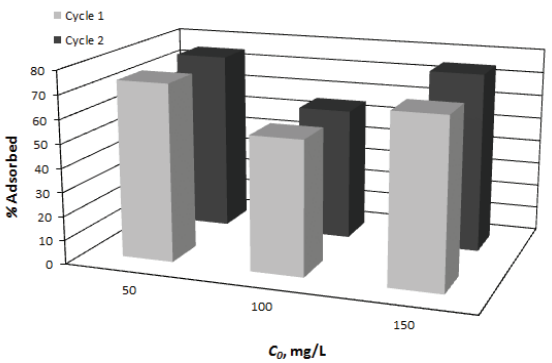

Fig. S1. Reactive black 5 dye adsorption-desorption cycles on α-cellulose/magnetite/polypyrrole composite.

where V_L is the liquid volume (mL), W_A is the adsorbent weight (g), ρ_p is the apparent density of the adsorbent particle (g mL^{-1}), k_f is the boundary layer mass transfer coefficient (m s^{-1}), R_o is the external composite radius (m), C is the dye concentration in the bulk liquid (mg L^{-1}), C_o is the dye concentration in the liquid within the adsorbent shell (mg L^{-1}), t is the time coordinate (s), and R in the radial coordinate (m).

In the composite shell a microscopic balance on the dye in the liquid results in Eq. (2). This balance considers temporal and radial variations of the dye concentration in the liquid within the shell, along with a dye transfer from the liquid to the surface of the shell.

$$\varepsilon_o \frac{\partial C_o}{\partial t} + \rho_o \frac{\partial Q_o}{\partial t} = D_o\left(\frac{\partial^2 C_o}{dR^2} + \frac{2}{R}\frac{\partial C_o}{\partial R}\right) \quad R_i \le R \le R_o \tag{2}$$

where ε_o is the shell porosity, ρ_o is the shell density (g mL^{-1}), D_o is the effective diffusivity of the dye in the shell (m^2 s^{-1}), R_i is the composite core radius (m), and Q_o is the dye concentration on the surface of the adsorbent (mg g^{-1} of shell).

A microscopic balance on the dye in the liquid results in Eq. (3). It is similar to Eq. (2) but with no possibility of adsorption.

$$\varepsilon_i \frac{\partial C_i}{\partial t} = D_i\left(\frac{\partial^2 C_i}{dR^2} + \frac{2}{R}\frac{\partial C_i}{\partial R}\right) \qquad 0 \le R \le R_i \tag{3}$$

where ε_i is the core porosity, D_i is the effective diffusivity in the core (m^2 s^{-1}), and C_i is the dye concentration in the liquid inside the adsorbent core.

Eq. (2) requires a constitutive equation to describe the adsorption process in terms C_o and Q_o. In this work a second order forward reaction (adsorption) and a first order backward (desorption) reaction were considered (Eq. (4)). At equilibrium, Eq. (4) reduces to the Langmuir isotherm (Eq. (5)).

$$\frac{\partial Q_o}{\partial t} = k_1 C_o\left(Q_m - Q_o\right) - k_2 Q_o \tag{4}$$

$$Q_{oe} = \frac{Q_m C_{oe}}{K_d + C_{oe}} \tag{5}$$

where k_1 is the forward rate constant (L mg·s^{-1}), k_2 is the backward rate constant (1 s^{-1}), K_d (k_2/k_1) is the equilibrium desorption constant (mg L^{-1}), Q_m is the maximum adsorption capacity for the shell (mg g^{-1}), C_{oe} is the dye concentration in the liquid within the adsorbent shell at equilibrium (mg L^{-1}), and Q_{oe} is the dye concentration in the surface of the adsorbent shell at equilibrium (mg g^{-1}).

The initial conditions for Eqs. (1)–(4) are reported in Eqs. (6)–(9). At the beginning, the dye molecules only exist in the bulk liquid.

$$C = C_A \tag{6}$$

$$C_i = 0, \qquad 0 \le R \le R_i \tag{7}$$

$$C_o = 0, \qquad R_i \le R \le R_o \tag{8}$$

$$Q_o = 0, \qquad R_i \le R \le R_o \tag{9}$$

where C_A is the initial dye concentration in the bulk liquid (mg L^{-1}). A no-flux condition at the center of the composite particles establishes the boundary condition given by Eq. (10).

$$R = 0, \qquad \frac{\partial C_i}{\partial R} = 0, \qquad t > 0 \tag{10}$$

A surface mass balance on the dye at the core/shell interface of the composite results in Eq. (11) (second boundary condition) establishes the continuity of the diffusion process when the dye molecules leave the shell and enter the core.

$$R = R_i, \qquad D_o \frac{\partial C_o}{\partial R} = D_i \frac{\partial C_i}{\partial R}, \qquad t > 0 \tag{11}$$

To complete the dye adsorption model, another surface mass balance on the dye at the surface of the composite results in Eq. (12). Similar to Eq. (1), it establishes the continuity of the convective flux (dye molecules crossing the boundary layer) with the diffusive flux (dye molecules entering the liquid inside the shell).

$$R = R_o, \qquad k_f\left(C - C_o\right) = D_o \frac{\partial C_o}{\partial R}, \qquad t > 0 \tag{12}$$

The mathematical model (Eqs. (1)–(12)) was set dimensionless by using the variables presented in Eqs. (13)–(16). Eq. (13) defines dimensionless dye concentrations in the bulk liquid, pores of the shell, and pores of the core. Eq. (14) defined dimensionless adsorbed dye concentration while Eq. (15) defines a dimensionless radial position. Finally, Eq. (16) defines the dimensionless temporal coordinate.

$$c = \frac{C}{C_A}, \qquad c_i = \frac{C_i}{C_A}, \qquad c_o = \frac{C_o}{C_A} \tag{13}$$

$$q_o = \frac{Q_o}{Q_m} \tag{14}$$

$$r = \frac{R}{R_o} \tag{15}$$

$$\tau = \frac{D_o t}{\varepsilon_o r_o^2} \tag{16}$$

The resulting dimensionless mathematical model is

$$\frac{dc}{d\tau} = -3N \left.\frac{\partial c_o}{\partial r}\right|_{r=1} \tag{17}$$

$$\frac{\partial c_o}{\partial \tau} + \xi \frac{\partial q_o}{\partial \tau} = \left(\frac{\partial^2 c_o}{dr^2} + \frac{2}{r}\frac{\partial c_o}{\partial r}\right) \qquad r_i \le r \le r_o \tag{18}$$

$$\frac{\partial c_i}{\partial \tau} = D\left(\frac{\partial^2 c_i}{dr^2} + \frac{2}{r}\frac{\partial c_i}{\partial r}\right) \qquad 0 \le r \le r_i \tag{19}$$

$$\frac{\partial q_o}{\partial \tau} = \varphi^2\left[\lambda c_o\left(1 - q_o\right) - q_o\right] \tag{20}$$

With initial conditions

$$c = 1 \tag{21}$$

$$c_i = 0, \qquad 0 \le r \le r_i \tag{22}$$

$$c_o = 0, \qquad r_i \le r \le r_o \tag{23}$$

$$q_o = 0, \qquad r_i \le r \le r_o \tag{24}$$

And boundary conditions

$$r = 0, \qquad \frac{\partial c_i}{\partial r} = 0, \qquad \tau > 0 \tag{25}$$

$$r = \frac{R_i}{R_o}, \qquad D_o \frac{\partial c_o}{\partial r} = D_i \frac{\partial c_i}{\partial r}, \qquad \tau > 0 \tag{26}$$

$$r = 1, \qquad \mathrm{Bi}\left(c - c_o\right) = \frac{\partial c_o}{\partial r}, \qquad \tau > 0 \tag{27}$$

Where the resulting dimensionless parameters are:

$$N = \frac{\varepsilon_o W_A}{V_L \rho_p}, \; \xi = \frac{\rho_o Q_m}{\varepsilon_o C_A}, \; D = \frac{\varepsilon_o D_o}{\varepsilon_i D_i}, \quad \varphi^2 = \frac{k_2 \varepsilon_o R_o^2}{D_o}, \; \lambda = \frac{C_A}{K_d}, \; \mathrm{Bi} = \frac{k_f R_o}{D_o} \tag{28}$$

3. Model solution and parameter estimation

The batch uptake kinetics mathematical model (Eqs. (17)–(20)) along with the initial and boundary conditions (Eqs. (21)–(27)) were solved using the method of lines.

The dimensionless radial coordinate was discretized using second-order finite differences. Integration in dimensionless time of the resulting ordinary differential equations was performed using stiff integrator ODE23s from Matlab. Batch dye uptake experiments were conducted to estimate adsorption isotherm parameters Q_m and K_d. The film mass transfer coefficient was calculated using the correlation by Geankoplis (Eq. (29)).

$$k_f = \frac{D_{AB}}{r_o} + 0.31\left(\frac{\mu_L}{\rho_L D_{AB}}\right)^{-2/3}\left(\frac{\Delta\rho\mu_L g}{\rho_L^2}\right)^{1/3} \quad (29)$$

where D_{AB} is the dye diffusivity ($m^2\ s^{-1}$), μ_L is the liquid viscosity (kg $m{\cdot}s^{-1}$), ρ_L is the liquid viscosity (kg/m^3), $\Delta\rho$ is the density difference ($\rho_p - \rho_L$) between the composite particle and the liquid (kg/m^3), and g is gravity acceleration (m/s^2). Dye diffusivity was estimated using the Wilke-Chang method according to the empirical modification of the Stokes-Einstein relation (Eq. (30)).

$$D_{AB} = \frac{7.4\times10^{-12}\left(\phi M_B\right)^{1/2} T}{\eta_B V_A^{0.6}} \quad (30)$$

where φ is the association factor of liquid (equal to 2.6 for water), M_B is the solvent molecular weight (g mol^{-1}), T is the temperature (K), V_A is the molar volume of dye at boiling temperature ($cm^3\ mol^{-1}$), and η_B is the solvent viscosity (cP). For the case of the studied dye, its molar volume was estimated using the method of Schroeder presented in Eq. (31).

$$V_A = 7(N_C + N_H + N_O + N_N + N_{DB}) + 24.5N_{Cl} + 21N_S - 7 \quad (31)$$

where N_C is the number of carbon atoms, N_H the number of hydrogen atoms, N_O the number of oxygen atoms, N_N the number of nitrogen atoms, N_{DB} the number of double bonds, N_{Cl} the number of chlorine atoms, and N_S the number of sulfur atoms.

The forward rate constant, k_1, was estimated by fitting experimental dye batch uptake data along with the dye effective diffusivity using fminsearch from Matlab. Both effective diffusivities, D_o and D_i, were considered as being equal for the sake of simplicity.

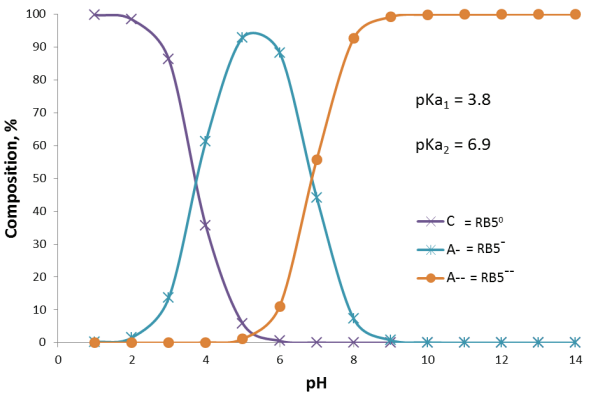

Fig. S2. Speciation diagram of reactive black 5 dye calculated using two pKa values.

4. Speciation diagram of reactive black 5 dye

Fig. S2 shows the speciation diagram of the reactive black 5 (also known as Remazol Black B) dye using two pKa values at 3.8 and 6.9 [43].

Fig. S3 shows the adsorption-desorption cycles of RB5 dye with different eluents such as NaOH, $Ca(OH)_2$, EDTA, HNO_3 all at a 0.1 M concentration aqueous solutions.

Table S1
Non-fitted parameters used in the mathematical model

Parameter	Value	Units
C_A	100	mg L^{-1}
V_L	30	mL
W_A	0.1	g
ρ_p	1.46	g mL^{-1}
ρ_o	1.45	g mL^{-1}
r_o	227.3×10^{-6}	m
r_i	212.5×10^{-6}	m
ε_o	0.35	
ε_i	0.28	
Q_m	260.7	mg g^{-1} shell
K_d	20.72	mg L^{-1}
N_C	26	
N_H	21	
N_N	5	
N_O	19	
N_{Cl}	0	
N_S	6	
N_{DB}	12	
V_A	700	$cm^3\ mol^{-1}$
Φ	2.6	
M_B	18	g mol^{-1}
T	298.15	K
η_B	1	cP
D_{AB}	2.96×10^{-10}	$m^2\ s^{-1}$
μ_L	0.001	kg $m^{-1}{\cdot}s$
ρ_L	1,000	kg/m^3
g	9.81	m/s^2
k_f	2.41×10^{-5}	m s^{-1}

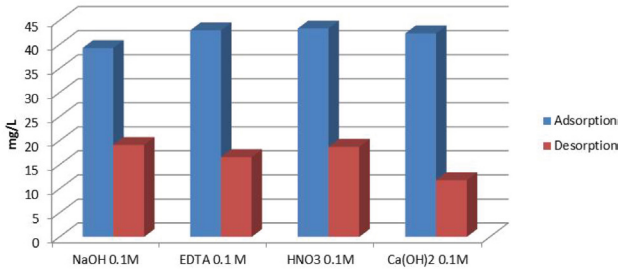

Fig. S3. Adsorption-Desorption cycles of RB5 dye on the composite using different eluents.